Biological Cybernetics manuscript No.
(will be inserted by the editor)

Magnus J. E. Richardson

Spike-train spectra and network response functions for non-linear integrate-and-fire neurons

Biological Cybernetics 99: 381-392 (2008)

Received: date / Revised: date

Abstract Reduced models have long been used as a tool for the analysis of the complex activity taking place in neurons and their coupled networks. Recent advanced in experimental and theoretical techniques have further demonstrated the usefulness of this approach. Despite the often gross simplification of the underlying biophysical properties, reduced models can still present significant difficulties in their analysis, with the majority of exact and perturbative results available only for the leaky integrate-and-fire model. Here an elementary numerical scheme is demonstrated which can be used to calculate a number of biologically important properties of the general class of non-linear integrate-and-fire models. Exact results for the first-passage-time density and spike-train spectrum are derived, as well as the linear response properties and emergent states of recurrent networks. Given that the exponential integrate-fire model has recently been shown to agree closely with the experimentally-measured response of pyramidal cells, the methodology presented here promises to provide a convenient tool to facilitate the analysis of cortical-network dynamics.

1 Introduction

Biophysically-detailed computational models and reduced mathematical models of neurons and networks provide complementary approaches to the understanding of the complex properties of neural tissue. Whereas the comparison of detailed models to experiment provides the ultimate test of a theoretical framework, reduced models allow for an analysis of the salient properties of neuronal function through their tractability and also provide an important guide for the computer-intensive large-scale simulations that constitute detailed modeling.

M.J.E. Richardson
Warwick Systems Biology Centre, University of Warwick, Coventry CV4 7AL, UK.
E-mail: magnus.richardson@warwick.ac.uk

A great variety of methods have been employed in the construction of reduced models. Recently, a rigorous approach to the evaluation of such models against experimental data (results from a recent competition are reported in Jolivet et al., 2008) has provided a renewed focus for the development of tractable models and their systematic biophysical refinement.

An important type of reduced spiking-neuron model is the integrate-and-fire class (see Burkitt 2006a 2006b and Lindner et al. 2004, for recent reviews) which is characterized by a threshold, whether at the putative beginning or peak of a spike, and a hard reset representing the effect of the inward-rectifier potassium channel (Hodgkin and Huxley 1952). A ubiquitous member of this class of model is the leaky IF (LIF) model, which features a linear, ohmic leak current and a threshold at the onset of the spike. Through the combination of such a dynamics with a model for stochastic synaptic drive (Stein 1965) it has been demonstrated that the LIF can provide a good fit to the average firing rates of cortical cells (Rauch et al. 2003) as well as the prediction of spike times (Paninski et al. 2004; Jolivet et al. 2006).

Non-linear integrate and fire models, like the quadratic IF (QIF) model (Brunel and Latham 2003), related to the canonical Type I theta-neuron model (Ermentrout and Kopell 1986) and the exponential IF (EIF) model introduced by Fourcaud-Trocmé et al. (2003) that captures the activation of the spike-generating sodium current, have also been analyzed. Such models have the potential to provide an even more accurate account of the properties of cortical neurons; and in fact it has recently been shown that the EIF model provides both an excellent fit to the current-voltage relation and accurate spike prediction for layer-5 somatosensory cortex pyramidal cells (Badel et al. 2008).

Despite their simplicity, the properties of non-linear IF neurons subject to stochastic synaptic drive are not always solvable in closed form. The steady-state firing rate has been provided for the LIF for both conductance (Johannesma 1968; Richardson 2004) and current-based input (Ricciardi et al. 1977) with solutions also pro-

vided for the QIF (Brunel and Latham 2003) and EIF (Fourcaud-Trocmé et al. 2003). In general the steady-state rate will take the form of the reciprocal of a double integral for any non-linear IF model, though further reduction is possible for the LIF (Brunel and Hakim 1999) under current-based synaptic fluctuations.

The time-dependent properties of IF models are considerably harder to derive, whether numerically or analytically, and this has hampered progress in the analysis of the dynamic properties of neurons and networks. Results exist for the LIF model; the linear response to current (Brunel and Hakim 1999) and noise (Brunel and Hakim 1999; Lindner et al. 2001; Silberberg et al. 2004) modulation, as well as the spike-train spectrum (Lindner et al. 2002). Some asymptotic results are also available for the response properties of the non-linear QIF and EIF (Fourcaud-Trocmé and Brunel 2005; Richardson 2007). Such time-dependent properties are central to the understanding of the dynamics of computations and emergent states possible in neural tissue. Moreover, recent experiments have directly probed these properties (Arsiero et al. 2007; Köndgen et al. 2008) and provide further potential for the biophysical refinement of the models.

Recently, a rather simple method for providing numerical solutions to the first-order response properties for the class of non-linear IF neuron models was introduced (Richardson 2007). The method involves separating the second-order Fokker-Planck differential equation, that results from the gaussian-white noise approximation to synaptic drive, into two first-order differential equations for the flux and probability density. The resulting equations can be solved, trivially, by integrating backwards from the threshold. Here, it will be shown that the threshold-integration method easily generalizes to other dynamic properties of IF models, such as the exact first-passage-time density, spike-triggered rate, propagator and spike-train spectrum. It can also be used to calculate the dynamical response of synaptically-coupled recurrent networks of neurons, either directly or by relation to the uncoupled network (Brunel and Wang 2003).

2 General theory

The voltage trajectories of neurons fluctuate under the influence of a stochastic synaptic input. The probability density $P(V,t)$, of finding a neuron near a voltage V at a time t, and the probability flux $J(V,t)$ passing through this voltage are related by the continuity equation

$$\frac{\partial P}{\partial t} + \frac{\partial J}{\partial V} = \text{initial conditions} + \text{sources} - \text{sinks} \qquad (1)$$

which is general for the class of IF models. The initial conditions can be written as delta-functions of time multiplying initial distributions, whereas the source (spike reset) and sink (spike threshold) can be written as delta-functions of voltage multiplying rate-like quantities. Written in this way, the initial and boundary conditions can be conveniently incorporated into the continuous description of the dynamics.

Stochastic dynamics of a single trajectory. The method developed in this paper is general for all non-linear IF neurons that have a dynamics of the form

$$\tau\frac{dV}{dt} = E(t) - V + \psi + \sigma\sqrt{2\tau}\xi(t) \qquad (2)$$

where τ is the membrane time constant, $E(t)$ is the instantaneous resting potential and ψ is some non-linear function of voltage that may model, for example, an explicit spike mechanism. For clarity a specific non-linear model is chosen as an illustration of the threshold integration method in the figures: the exponential IF (EIF) model. This was introduced on theoretical grounds in Fourcaud-Trocmé et al. (2003) and recently (Badel et al. 2008) shown experimentally to provide a close fit to the response properties of somatosensory-cortex, layer-5 pyramidal cells. The form of ψ in this case is

$$\psi(V) = \Delta_T e^{(V-V_T)/\Delta_T}. \qquad (3)$$

The onset of the spike is parameterized by V_T and has a sharpness Δ_T. The spike is terminated at some threshold voltage V_{th} (at which $P(V_{th})=0$) with the neuron then refractory for a period τ_r before being reinserted at a reset potential V_{re} (the fall of the spike takes place in the refractory period - see Appendix). Because of this, the probability density must be separated into a component P that evolves under the continuous dynamics, and a component that is refractory, The correct normalization for P is therefore

$$\int_{V_{lb}}^{V_{th}} P(V,t)dV + \int_{t-\tau_r}^{t} dt' r(t') = 1 \qquad (4)$$

where $r(t)$ is the instantaneous firing rate at a time t. The remaining terms in equation (2) concern the synaptic fluctuations: σ is the voltage standard deviation (in the absence of a spiking mechanism); and $\xi(t)$ is a zero-mean, delta-correlated $\langle\xi(t)\xi(t')\rangle = \delta(t-t')$ gaussian white noise term.

The flux J. With the dynamics in equation (2) the flux appearing in the continuity equation (1) can be shown (Risken 1996) to be

$$\tau J = (E(t) + \psi - V)P - \sigma^2\frac{\partial P}{\partial V}. \qquad (5)$$

It should be noted that this equation, by virtue of the gaussian white-noise term, features a derivative of the probability P with respect to voltage. It is this feature, together with the derivative of the flux with respect to voltage in equation (1) that underpins the threshold integration method. The firing rate $r(t)$ is the flux at threshold $J(V_{th},t)$.

A lower bound on the voltage A lower bound V_{lb} on the voltage is also added in the form of a zero-flux criterion

$$J(V_{lb}, t) = 0. \tag{6}$$

The value of V_{lb} is chosen to be sufficiently negative ($V_{lb} = -100\text{mV}$) so that its exact value does not impact significantly on the observable dynamics. It can be noted that a more depolarized value for such a zero-flux condition has been suggested (Lansky and Lanska 1987; Rauch et al. 2003) as an approximation to the effects of the inhibitory synaptic-reversal potential.

3 Uncoupled populations of neurons

The case of an uncoupled population of identical neurons, receiving independent sources of synaptic fluctuations, is first considered. The density and flux can therefore be interpreted either as representing the states of a fraction of neurons across the population ensemble, or probabilistically in the context of single-neuron dynamics. Exact results for the steady-state density, first-passage-time density, spike-triggered rate and spectrum are first derived in sections 3.1-3.2, followed by the first-order, linear response to current modulation in section 3.3.

3.1 Steady-state properties

The steady-state rate of non-linear IF neurons can be found in closed analytical form in terms of the reciprocal of a double integral (which, nevertheless, must be evaluated numerically) as has been already discussed. The steady-state rate is therefore a good starting point for the introduction of the numerical threshold integration method and also provides a very convenient numerical scheme for the calculation of steady-state rates for IF models that is at least equivalent in its simplicity to evaluating the closed-form, double-integral solution.

In the steady state the continuity equation (1) and flux equation (5) can be re-arranged to provide two first-order linear differential equations for the flux J_0 and probability density P_0, respectively

$$-\frac{\partial J_0}{\partial V} = r_0\delta(V - V_{th}) - r_0\delta(V - V_{re}) \tag{7}$$

$$-\frac{\partial P_0}{\partial V} = \frac{1}{\sigma^2}\left(\tau J_0 + (V - E_0 - \psi)P_0\right) \tag{8}$$

implying that the boundary conditions are $P_0(V_{th}) = 0$ and $J_0(V_{th}) = r_0$. The firing rate r_0 is unknown, but can be scaled out by the substitutions $J_0 = r_0 j_0$ and $P_0 = r_0 p_0$ to reduce the equations to the form

$$-\frac{\partial j_0}{\partial V} = \delta(V - V_{th}) - \delta(V - V_{re}) \tag{9}$$

$$-\frac{\partial p_0}{\partial V} = \frac{1}{\sigma^2}\left(\tau j_0 + (V - E_0 - \psi)p_0\right) \tag{10}$$

implying that the conditions are now $p_0(V_{th}) = 0$ and $j_0(V_{th}) = 1$. These equations can be numerically integrated from threshold V_{th} to the lower bound V_{lb} to yield j_0 and p_0 (see the Appendix for a convenient scheme). These in turn give the firing rate r_0 from the normalization condition in equation (4):

$$r_0 = \left(\int_{V_{lb}}^{V_{th}} p_0(V)dV + \tau_r\right)^{-1}. \tag{11}$$

In figure 1A the firing rate as a function of resting potential E_0 is plotted for three different fluctuation strengths. Two examples are chosen to illustrate the methods in this paper; a quasi-deterministic, suprathreshold firing regime and a fluctuation-driven subthreshold firing regime. The steady-state, piece-wise constant flux and probability density, corresponding to these two examples, is plotted in figure 1B and example trajectories from simulations of equation (2) are provided in figures 1C and 1D.

3.2 First-passage time, propagator and spike spectrum

First-passage-time density. A dynamic quantity, the first-passage-time (FTP) density is now considered. Here, the initial distribution at time t_0 is chosen to be a delta function centered at V_0. However, the method described works equally well if an arbitrary initial distribution is chosen instead. The time-dependent continuity (1) and flux (5) equations, corresponding to the absorbing boundary at threshold and this choice of initial conditions, are

$$-\frac{\partial J}{\partial V} = \frac{\partial P}{\partial t} + f(t)\delta(V - V_{th}) - \delta(t - t_0)\delta(V - V_0) \tag{12}$$

$$-\frac{\partial P}{\partial V} = \frac{1}{\sigma^2}\left(\tau J + (V - E_0 - \psi)P\right). \tag{13}$$

The first-passage time density $f(t) = J(V_{th}, t)$ is equivalent to the time-dependent flux at threshold. The equations are then fourier-transformed over time (see Appendix for convention)

$$-\frac{\partial \widetilde{J}}{\partial V} = i\omega\widetilde{P} + \widetilde{f}\delta(V - V_{th}) - e^{-i\omega t_0}\delta(V - V_0) \tag{14}$$

$$-\frac{\partial \widetilde{P}}{\partial V} = \frac{1}{\sigma^2}\left(\tau\widetilde{J} + (V - E_0 - \psi)\widetilde{P}\right). \tag{15}$$

These equations feature two inhomogeneous terms (the threshold and initial conditions) and can be solved by separating the solution into two parts:

$$\widetilde{P} = \widetilde{f}\widetilde{p}_f + \widetilde{p}_0 \quad \text{and} \quad \widetilde{J} = \widetilde{f}\widetilde{\jmath}_f + \widetilde{\jmath}_0 \tag{16}$$

where $\widetilde{p}_f$ and $\widetilde{\jmath}_f$ deal with the absorbing boundary condition at V_{th}

$$-\frac{\partial \widetilde{\jmath}_f}{\partial V} = i\omega\widetilde{p}_f + \delta(V - V_{th}) \tag{17}$$

$$-\frac{\partial \widetilde{p}_f}{\partial V} = \frac{1}{\sigma^2}\left(\tau\widetilde{\jmath}_f + (V - E_0 - \psi)\widetilde{p}_f\right) \tag{18}$$

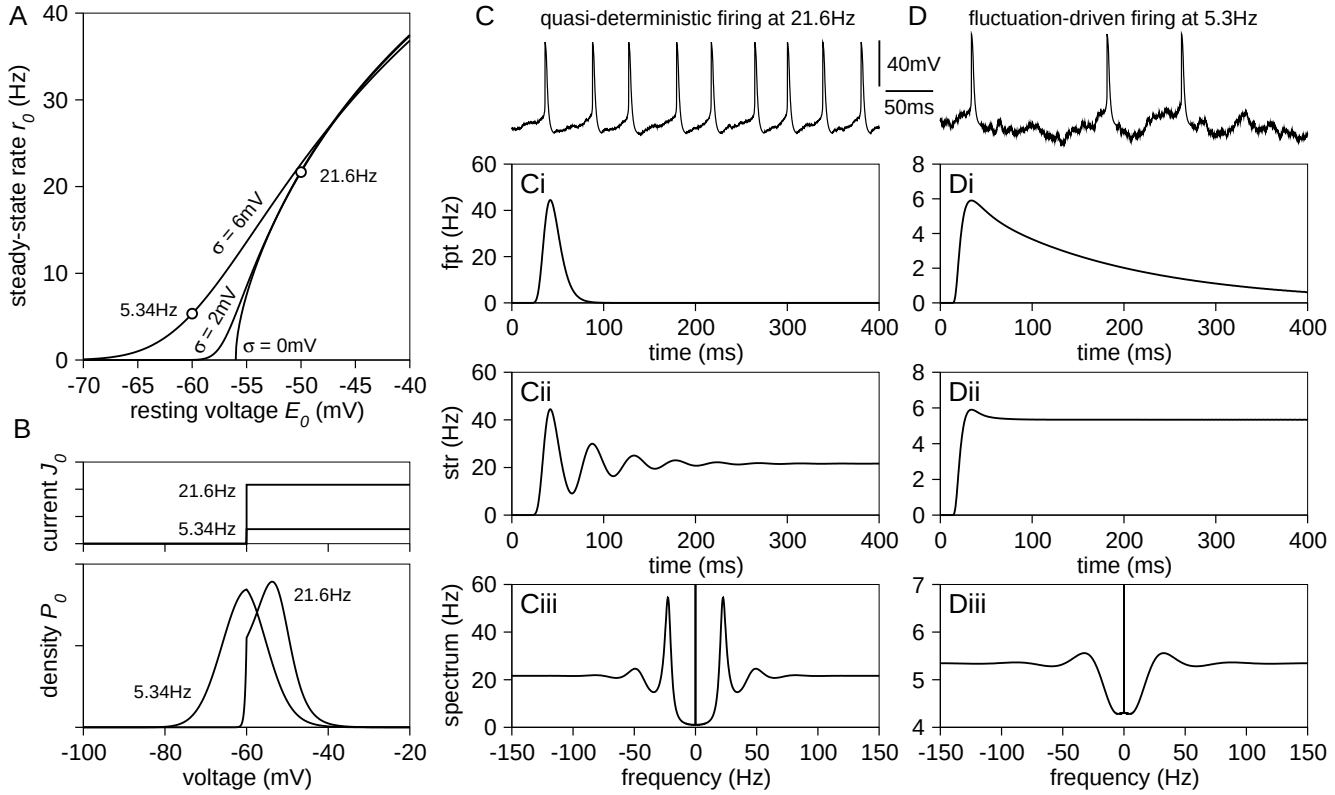

Fig. 1 Exact numerical results for the exponential integrate-and-fire (EIF) model with a refractory period $\tau_r = 10$ms; (A) The steady-state firing rate r_0 derived from Eqs. 7,8 for three fluctuation strengths ($\sigma = 0$, 2 and 6mV). Two example cases are identified (open circles): quasi-deterministic, suprathreshold firing ($E_0 = -50$mV, $\sigma = 2$mV); and fluctuation-driven, subthreshold firing ($E_0 = -60$mV, $\sigma = 6$mV). (B) The steady-state flux J_0 (a piece-wise constant) and probability density P_0 for these two cases. (C) Example voltage trace from a simulation of Eq. 2 for quasi-deterministic firing: (Ci) First-passage time density FPT from the inverse transform of the solution to Eqs. 14,15; (Cii) Spike-triggered rate STR from the inverse transform of the solution to Eq. 23; and (Ciii) Spike-train power-spectrum calculated using the STR and Eq. 28. (D) Example voltage trace for fluctuation-driven firing: (Di) FPT; (Dii) STR; and (Diii) Spike-train power-spectrum. For this, and all other figures, the parameters were $\tau = 20$ms, $\Delta_T = 3$mV, $V_T = -53$mV, $V_{th} = 20$mV and $V_{re} = -60$mV (see Appendix for further details). The exact solutions were integrated backwards from threshold with a time step $\Delta V = 10\mu$V (an algorithm is provided in the Appendix).

implying that $\widetilde{p}_f(V_{th}) = 0$ and $\widetilde{j}_f(V_{th}) = 1$ and where $\widetilde{p}_0$ and $\widetilde{j}_0$ (not to be confused with the steady-state solutions of the previous section) account for the initial conditions

$$-\frac{\partial \widetilde{j}_0}{\partial V} = i\omega \widetilde{p}_0 - e^{-i\omega t_0}\delta(V - V_0) \tag{19}$$

$$-\frac{\partial \widetilde{p}_0}{\partial V} = \frac{1}{\sigma^2}\left(\tau \widetilde{j}_0 + (V - E_0 - \psi)\widetilde{p}_0\right) \tag{20}$$

implying that $\widetilde{p}_0(V_{th}) = 0$ and $\widetilde{j}_0(V_{th}) = 0$. The two of pairs of equations (17,18) and (19,20) can be solved numerically by simultaneously integrating them from threshold V_{th} to the lower bound V_{lb} (see Appendix for further details) as was done for the steady-state case. However, for the FPT density the unknown multiplier $f(\omega)$ is found from the zero-flux condition (6) which when applied to the flux $\widetilde{J}$ of equation set (16) yields

$$\widetilde{f}(\omega) = -\widetilde{j}_0(V_{lb})/\widetilde{j}_f(V_{lb}). \tag{21}$$

The fourier transform of the FPT density can be directly used to find the spike-train spectrum. However, if the real-time FPT is required then equation (21) can be inverse-transformed; in figure 1Ci and 1Di the FPT densities for the non-linear exponential IF neuron are shown for the quasi-deterministic and fluctuation-driven firing regimes.

It can be noted that this method allows the spike-train CV for any non-linear integrate-and-fire neuron to be calculated, generalising the results for the linear, leaky IF model (Lindner et al. 2003).

Spike-triggered-rate density. A quantity closely related to the FPT is the spike-triggered-rate density (STR) $\rho(t)$. This is defined as the time-dependent firing rate of the population, starting from some specified initial distribution, and where the full neuronal dynamics with reset are included. The difference to the FPT is therefore that, post-spike, the neuron is reinserted at V_{re} after the refractory period has ended. For renewal processes (Gerstner and Kistler 2002) the FPT and STR are related by a series of nested convolutions which, on fourier transfor-

mation, lead to a power series that may be solved giving the relation

$$\widetilde{\rho}(\omega) = \widetilde{f}(\omega)/(1-\widetilde{f}(\omega)) \tag{22}$$

unless $\omega = 0$, in which case $\rho(0) = \pi r_0 \delta(\omega)$. However, the STR can also be calculated directly by simply modifying equation (12) to include the reset

$$-\frac{\partial J}{\partial V} = \frac{\partial P}{\partial t} + \rho(t)\delta(V-V_{th}) - \rho(t-\tau_r)\delta(V-V_{re}) - \delta(t-t_0)\delta(V-V_0). \tag{23}$$

A natural choice for the initial condition is $t_0 = \tau_r$ (the step required to fully implement the refractory period for the STR calculation) and $V_0 = V_{re}$ corresponding to a spike at $t = 0$. The fourier transform of (23), and the related equation for P, can be taken, and a similar strategy of separating the solution into two parts employed:

$$\widetilde{P} = \widetilde{p}_0 + \widetilde{\rho}\widetilde{p}_\rho \quad \text{and} \quad \widetilde{J} = \widetilde{\jmath}_0 + \widetilde{\rho}\widetilde{\jmath}_\rho \tag{24}$$

with the equation analogous to (17) for $\widetilde{\jmath}_\rho$ taking the form

$$-\frac{\partial \widetilde{\jmath}_\rho}{\partial V} = i\omega\widetilde{p}_\rho + \delta(V-V_{th}) - e^{-i\omega\tau_r}\delta(V-V_{re}) \tag{25}$$

so $\widetilde{p}_\rho(V_{th}) = 0$ and $\widetilde{\jmath}_\rho(V_{th}) = 1$. On applying the zero-flux condition, the fourier transform of the STR is found from $\rho(\omega) = -\widetilde{\jmath}_0(V_{lb})/\widetilde{\jmath}_\rho(V_{lb})$. The real-time STR densities for the two example firing regimes are plotted in figure 1Cii and 1Dii. It can be noted that this method also yields a simple numerical solution to finding the propagator for non-linear IF neurons, which is the probability density of finding the neuron near a voltage V at a time t, given some sharp initial condition V_0, t_0.

Spike-train power spectrum. The STR density is directly related to the auto-correlation $C(T)$ of the spike-train

$$C(T) = \langle S(t)S(t+T)\rangle = r_0\delta(T) + r_0\rho(|T|) \tag{26}$$

where $S(t) = \sum_{\{t_k\}}\delta(t-t_k)$ is the delta-function spike train (Gerstner and Kistler 2002). The spike-train power spectrum, an important temporal measure of the structure of activity in the steady-state population, is given by the fourier transform of $C(T)$

$$\widetilde{C}(\omega) = \int_{-\infty}^{\infty} dT e^{-i\omega T} C(T). \tag{27}$$

This can be rewritten as

$$\widetilde{C}(\omega) = r_0\left(1 + \widetilde{\rho}(\omega) + \widetilde{\rho}(-\omega)\right) = r_0\left(1 + 2\Re\left[\widetilde{\rho}(\omega)\right]\right). \tag{28}$$

The integration method applied to the STR therefore provides a convenient scheme for calculating the power spectra of populations of non-linear IF neurons. The spectra for the two firing regimes, quasi-deterministic and fluctuation driven, are plotted in figures 1Ciii and 1Diii, respectively.

3.3 Linear response to parameter modulations

The response of populations of IF neurons to various parameter modulations (current, conductance, noise amplitude, etc) was treated in detail in Richardson (2007). Here results for current modulation, equivalent to modulation of the instantaneous resting potential $E(t)$, are reviewed and generalised to the refractory case. These equations will provide the basis for the network response to modulation that is treated in the next section.

A scenario is considered in which a parameter α is modulated harmonically $\alpha = \alpha_0 + \alpha_1 e^{i\omega t}$. The aim is to derive the induced modulation of the flux, probability density and firing rate to first (linear) order in the modulation strength α_1. In this case the solution is of the form

$$J = J_0 + \hat{J}_\alpha e^{i\omega t} \quad \text{and} \quad P = P_0 + \hat{P}_\alpha e^{i\omega t} \tag{29}$$

where J_0, P_0 are the steady-state flux and probability density of equations (7,8) with the refractory condition of equation (4), and $\hat{J}_\alpha$ and $\hat{P}_\alpha$ are the first-order response to be determined. The firing rate modulation $r = r_0 + \hat{r}_\alpha e^{i\omega t}$ is expanded similarly and given by the flux at threshold.

Response to current modulation. The modulated resting potential takes the form $E(t) = E_0 + E_1 e^{i\omega t}$ and so the linear response, from equation (1) and the expansion of equation (5) to first order, must satisfy

$$-\frac{\partial \hat{J}_E}{\partial V} = i\omega\hat{P}_E + \hat{r}_E\delta(V-V_{th}) - \hat{r}_E e^{-i\omega\tau_r}\delta(V-V_{re}) \tag{30}$$

$$-\frac{\partial \hat{P}_E}{\partial V} = \frac{1}{\sigma^2}\left(\tau\hat{J}_E + (V-E_0-\psi)\hat{P}_E - E_1P_0\right) \tag{31}$$

implying $\hat{P}_E(V_{th}) = 0$ and $\hat{J}_E(V_{th}) = \hat{r}_E$. The method of separating the solutions into two parts is applied, one proportional to $\hat{r}_E$ and a second to E_1

$$\hat{P}_E = \hat{r}_E\hat{p}_r + E_1\hat{p}_E \quad \text{and} \quad \hat{J}_E = \hat{r}_E\hat{\jmath}_r + E_1\hat{\jmath}_E \tag{32}$$

which yield the pairs of equations

$$-\frac{\partial \hat{\jmath}_r}{\partial V} = i\omega\hat{p}_r + \delta(V-V_{th}) - e^{-i\omega\tau_r}\delta(V-V_{re}) \tag{33}$$

$$-\frac{\partial \hat{p}_r}{\partial V} = \frac{1}{\sigma^2}\left(\tau\hat{\jmath}_r + (V-E_0-\psi)\hat{p}_r\right). \tag{34}$$

implying the conditions $\hat{p}_r(V_{th}) = 0$ and $\hat{\jmath}_r(V_{th}) = 1$, and

$$-\frac{\partial \hat{\jmath}_E}{\partial V} = i\omega\hat{p}_E \tag{35}$$

$$-\frac{\partial \hat{p}_E}{\partial V} = \frac{1}{\sigma^2}\left(\tau\hat{\jmath}_E + (V-E_0-\psi)\hat{p}_E - P_0\right). \tag{36}$$

so that $\hat{p}_E(V_{th}) = 0$ and $\hat{\jmath}_E(V_{th}) = 0$. Again, these can be solved numerically by integrating from the threshold V_{th} to the lower bound V_{lb} and then applying a zero-flux criterion $\hat{J}_E(V_{lb}) = 0$. This gives the linear-response rate amplitude as

$$\hat{A}_E(i\omega) = -\hat{\jmath}_E(V_{lb})/\hat{\jmath}_r(V_{lb}) \quad \text{so} \quad \hat{r}_E = E_1\hat{A}_E. \tag{37}$$

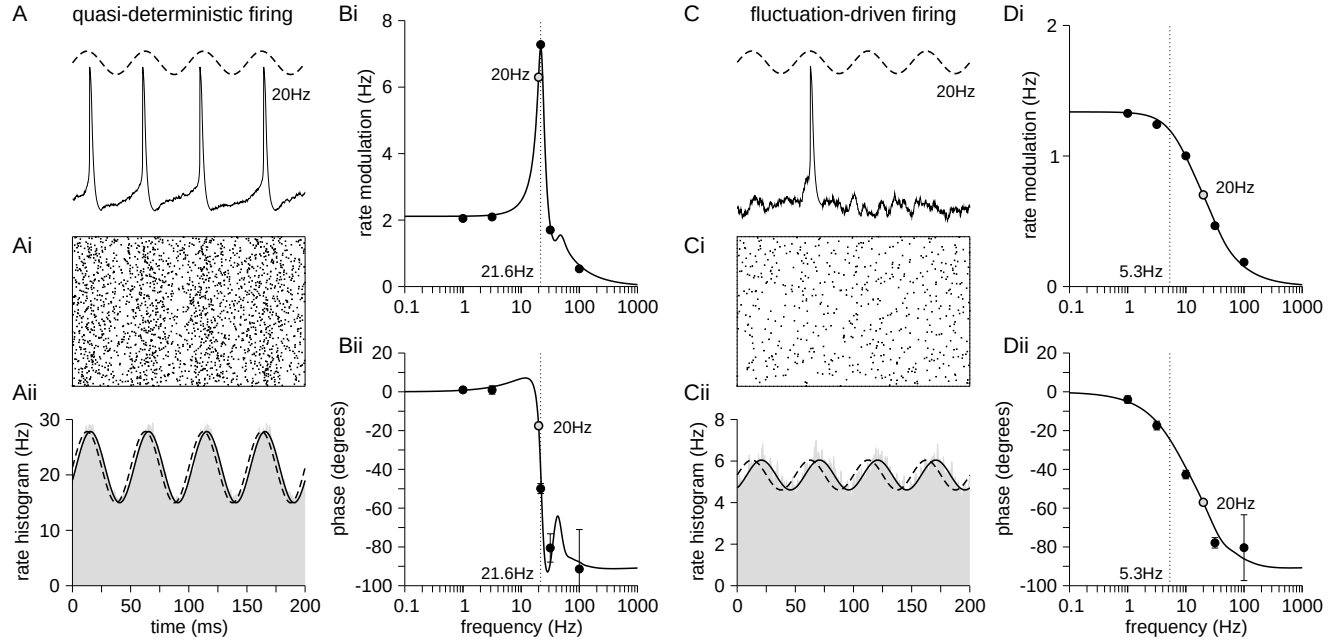

Fig. 2 First-order dynamic response of an uncoupled population of EIF neurons to current modulation. (A) Case of quasi-deterministic firing at $r_0 = 21.6$Hz. The action-potentials appear on average near the peak of the modulated current of amplitude $E_1 = 1$mV and frequency 20Hz (illustrated by dashed line). (Ai) Raster plot of 500 neurons with the rate modulation clearly visible. (Aii) Histogram of spike times (grey) showing sinusoidal modulation $\hat{r}_E$ (black line) from which the amplitude and phase advance from the input current (dashed line, shown with same amplitude for phase comparison) can be measured. (Bi) The amplitude $|\hat{r}_E|$ and (Bii) phase advance of $\hat{r}_E$ for the quasi-deterministic case calculated from Eqs. 33-36. The first-order linear amplitude and phase response (solid lines) are in good agreement with simulations of the full model (black circles). The points corresponding to 20Hz modulation are also marked (open circles). (C) Fluctuation-driven firing at $r_0 = 5.3$Hz with a current modulation $E_1 = 1$mV at frequency 20Hz. (Ci) Raster plot for 500 neurons. (Cii) Histogram and extraction of amplitude and phase. A phase delay is clearly seen. (Di) The amplitude $|\hat{r}_E|$ and (Dii) phase for the fluctuation-driven case. The EIF parameters correspond to those given in Fig. 1.

Figure 2 shows the calculated response properties for the quasi-deterministic (2A and 2B) and fluctuation-driven (2C and 2D) firing regimes. Panel 2Ai shows an example trajectory over four complete periods. The modulation frequency (20Hz) is close to the steady-state firing rate for this case ($r_0 = 21.6$Hz) and the neuron fires near the peak modulation, though with some scatter as can be seen in the raster plot of figure 2Aii and the histogram 2Aiii. At this frequency the response (bold line) weakly lags behind the modulation (dashed lines). Panels 2Bi and 2Bii show the amplitude and phase of the theoretical rate modulation (Eq. 37) as a function of the modulation frequency. As expected (Knight 1972a,b) in this low-noise regime a strong resonance is visible when the modulation frequency is near the steady-state rate $r_0 = 21.6$Hz (dashed line). For the case of fluctuation-driven firing (steady-state rate $r_0 = 5.3$Hz) the response to modulation is weaker and shows a longer phase lag at 20Hz (panel 2Cii). As expected for this fluctuation-dominated case, there is no resonance in the amplitude in panel 2Di, nor is there a phase zero in the phase response (2Dii).

4 Recurrent networks of non-linear IF neurons

The theoretical framework required for the treatment of recurrent neural networks, particularly for those that undergo an oscillatory transition, is well developed for networks of LIF neurons (Brunel and Hakim 1999; Brunel and Wang 2003). It will now be demonstrated, using a recurrent inhibitory network of delay-coupled EIF neurons with synaptic filtering, that the integration method can be readily adapted to deal with the response properties of neural networks, their eigenmodes and diagrams of emergent states.

Network structure. A recurrent, inhibitory network is considered which receives an afferent excitatory drive providing a resting potential E_0 and fluctuations parameterized by σ. These dynamics (contained in Eq. 2) are supplemented by a mean-field network coupling, parameterized by a strength $E_s < 0$ in units of voltage. The total instantaneous resting potential $E(t)$ therefore becomes

$$E(t) = E_0 + E_s S(t) \quad \text{where} \quad \tau_s \frac{dS}{dt} = \tau_s r(t - \tau_d) - S. \quad (38)$$

The differential equation for S allows for synaptic filtering τ_s and an axonal delay τ_d to be included (Brunel

and Wang 2003). To ease comparison with the uncoupled population, quantities x that are associated with the network case will be dashed x'. Before continuing, it should be noted that the current-based synaptic coupling is chosen here purely for reasons of methodological clarity. This is not a complete model of synaptic drive, particularly for the case of inhibition, as the potentially significant shunting conductance component is ignored. However, as shown in Richardson (2007) the effects of conductance modulation can be easily incorporated in the threshold integration method - a point that is returned to in the Discussion section.

The steady-state network rate. The method for finding the steady-state rate for mean-field networks follows the standard self-consistent approach. In the steady state the rate is constant $S_0 = \tau_s r'_0$ and so an effective resting potential can be defined $E'_0 = E_0 + E_s\tau_s r'_0$ from equation (38). The firing rate, parameterized by the unknown E'_0, can be calculated from the uncoupled network equations (7,8) with E_0 replaced by E'_0. A second equation for the firing rate can be found by re-arranging the equation for the effective resting potential

$$r'_0 = (E'_0 - E_0)/E_s\tau_s. \tag{39}$$

The firing rate of the network r'_0 is then found by plotting the two forms of the firing rate as a function of E'_0 with the intersections providing the set of fixed points. For the case of inhibition considered here $E_s < 0$ and only one fixed point is possible. This construction is illustrated in figure 3A for a number of different coupling strengths E_s and resting potentials E_0 such that the resulting effective resting potential E'_0 yields an inhibitory network of firing rate 5.3Hz. This choice has been taken so that comparison can be made with the fluctuation-driven firing case treated in the previous sections on uncoupled networks.

4.1 Response of a recurrent network to modulation

It is now considered that the afferent excitatory drive received by the recurrent network features a component that is sinusoidally modulated, so that the instantaneous resting potential of a neuron in the network can be written

$$E(t) = E_0 + E_s S(t) + E_1 e^{i\omega t}. \tag{40}$$

To first order, this will induce a modulation in the network rate $r'(t) = r'_0 + \hat{r}'_E e^{i\omega t}$ and synaptic parameter $S(t)$ so that

$$S(t) = S_0 + \hat{s}\hat{r}'_E e^{i\omega t} \quad \text{where} \quad \hat{s} = \tau_s \frac{e^{-i\omega\tau_d}}{1 + i\omega\tau_s} \tag{41}$$

where the second result comes from the Fourier transform of the differential equation (38). The network modulation equations, analogous to (30,31) therefore take the form

$$-\frac{\partial \hat{J}'_E}{\partial V} = i\omega\hat{P}'_E + \hat{r}'_E\delta(V - V_{th}) - \hat{r}'_E e^{-i\omega\tau_r}\delta(V - V_{re}) \tag{42}$$

$$-\frac{\partial \hat{P}'_E}{\partial V} = \frac{1}{\sigma^2}\Big(\tau\hat{J}'_E + (V - E'_0 - \psi)\hat{P}'_E - (E_1 + \hat{r}'_E E_s\hat{s})P'_0\Big) \tag{43}$$

where P'_0 is the steady-state probability density calculated from equation set (7,8) with E_0 replaced by E'_0. The equations above are again solved by separating solutions into one that is proportional to $\hat{r}'_E$ and a second to E'_1

$$\hat{P}'_E = \hat{r}'_E\hat{p}'_r + E_1\hat{p}'_E \quad \text{and} \quad \hat{J}'_E = \hat{r}'_E\hat{\jmath}'_r + E_1\hat{\jmath}'_E. \tag{44}$$

This results in two pairs of equations, identical to the modulation for the uncoupled population (33,34) and (35,36) except that the equation analogous to (34) for $\hat{p}'_r$ now becomes

$$-\frac{\partial \hat{p}'_r}{\partial V} = \frac{1}{\sigma^2}\left(\tau\hat{\jmath}'_r + (V - E_0 - \psi)\hat{p}'_r - E_s\hat{s}P'_0\right). \tag{45}$$

These equations can then be integrated backwards from V_{th} to V_{lb}, with the network response to modulation extracted from the zero-flux condition

$$\hat{r}'_E = -E_1\hat{\jmath}'_E(V_{lb})/\hat{\jmath}'_r(V_{lb}). \tag{46}$$

Examples of the network response are provided in figure panels 3Bi-Biv. As the synaptic coupling becomes stronger (more negative, for this inhibitory network) a network resonance develops that is not present in the uncoupled case (see panel 2Di). Simulations of the mean rate over the network are provided in panels 3Ci-Civ in which damped oscillations of increasing persistence are seen. The ratio of the amplitudes of peak-rate response (at resonance) to the response at zero frequency are plotted in panel 3D. This ratio diverges at a coupling strength of $E^*_s\tau_s r'_0 = -20.3$mV for the fluctuation-driven firing case with $r'_0 = 5.3$Hz.

Relation to the uncoupled network. The method just described provides a direct route to the network modulation. However, the solution can also be related to the that of the uncoupled population. This can be seen in equation (43) where an effective modulation strength $E'_1 = E_1 + \hat{r}'_E E_s\hat{s}$ can be identified. This brings the form of the network equations into that of the uncoupled population, which is known to have a response of the form given in equation (37). Hence, $\hat{r}'_E = E'_1\hat{A}_E$ where here $\hat{A}_E$ is calculated using $E_0 \to E'_0$. By combining the last two equalities, by substituting for E'_1, the following result is found

$$\hat{r}'_E = E_1\hat{A}_E/(1 - E_s\hat{s}A_E). \tag{47}$$

This relation between the uncoupled population and coupled network can also be seen by comparing the structure of equation pairs (30,31) and (42,43). Instead of the substitution (44) the substitution $\hat{J}'_E = \hat{r}'_E\hat{\jmath}_r + E_1\hat{\jmath}_r + \hat{r}'_E E_s\hat{s}\hat{\jmath}_E$ could be constructed, where $\hat{\jmath}_r$ and $\hat{\jmath}_E$ are the

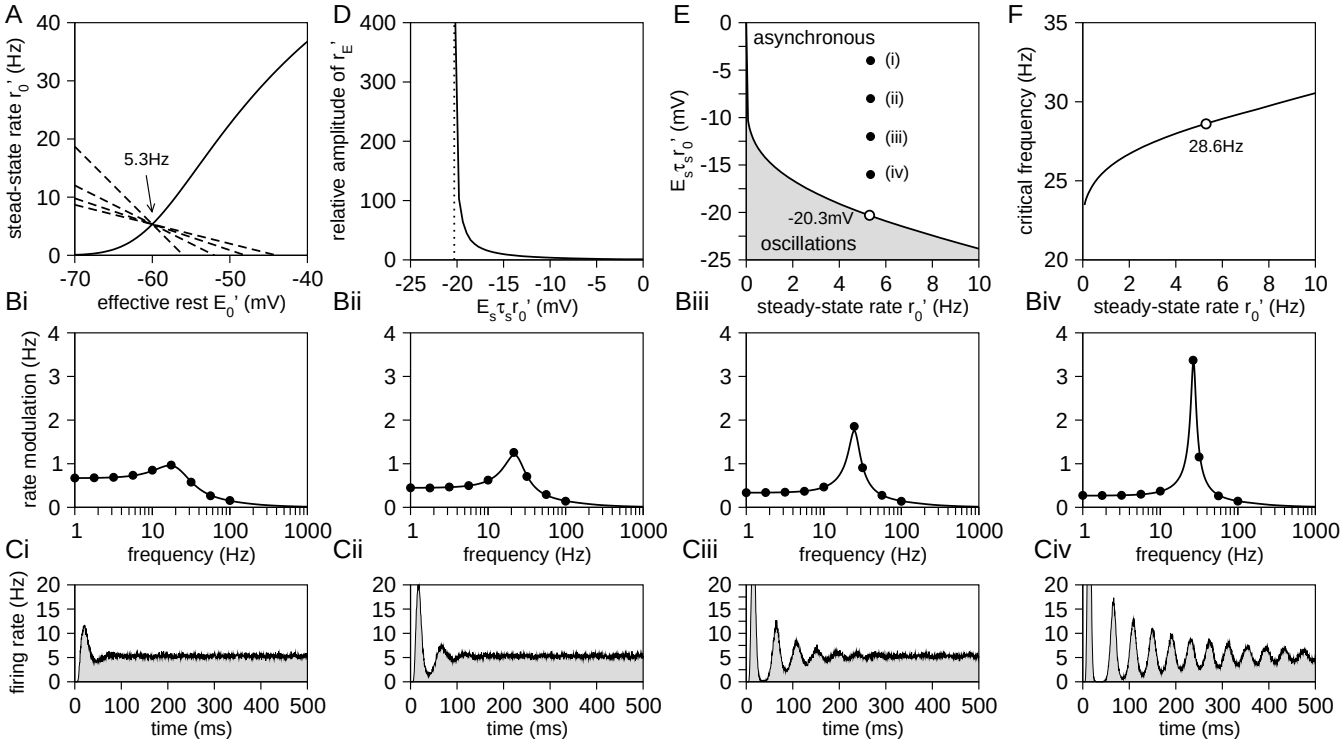

Fig. 3 Response properties and phase diagram for an inhibitory network of EIF neurons with synaptic time constant $\tau_s = 10$ms and axonal delay $\tau_d = 5$ms (please see Fig. 1 for other parameter values). (A) Construction of the self-consistent solution for the steady-state firing rate r_0' of the network. The firing rate of the uncoupled network (solid line) as a function of the effective resting potential E_0'. The intersection with Eq. 39 (dashed lines) gives the network rate r_0'. Four different coupling strengths E_s are considered ($E_s\tau_s r_0' = -4, -8, -12, -16$mV with compensatory resting potentials $E_0 = -56, -52, -48, -44$mV altered such that the network firing rate remains at $r_0' = 5.3$Hz. (Bi-Biv) the corresponding network response to modulation by an external signal of strength $E_1 = 1$mV. A resonance (not present in the uncoupled case of Fig 2Di) develops with an amplitude growing with the coupling strength. Close agreement is seen between the solutions to the first-order response theory given by Eqs 42,43 (solid line) and simulations of the full mode (black circles). (Ci-Civ) A simulation of the network dynamics from an initial refractory state, demonstrating the emergence and strengthening of damped oscillations with increasing inhibitory feedback. (D) Ratio of response at resonant peak to that at zero frequency (for each coupling strength) as a function of the inhibitory coupling. The amplitude diverges near a critical value $E_s^*\tau_s r_0' = -20.3$mV because the response to modulation at the resonance frequency goes to infinity at the transition to spontaneous oscillations. (E) Phase diagram for the inhibitory EIF network showing the line of critical coupling strength upon which the lowest eigenvalue becomes purely imaginary, as a function of the steady-state rate r_0'. The points (i)-(iv) marked for the case when $r_0' = 5.3$Hz correspond to the panels B and C. For $r_0' = 5.3$Hz the transition occurs at a synaptic strength $E_s^*\tau_s r_0' = -20.3$mV (open circle). (F) Critical frequency on the transition line. For $r_0' = 5.3$Hz (open circle) at the critical point oscillations emerge with a frequency of 28.6Hz.

solutions for an uncoupled population (but with E_0 replaced by E_0'). Then the zero-flux condition at V_{lb} gives

$$\hat{r}_E' = -E_1\hat{j}_E(V_{lb})/(\hat{j}_r(V_{lb}) + E_s\hat{s}\hat{j}_E(V_{lb})). \tag{48}$$

On dividing both numerator and denominator on the right-hand side by $\hat{j}_r(V_{lb})$, and using the result in equation (37), equation (47) is again found.

4.2 Network modes and phase diagrams

The framework required to extract the eigenmodes of the network dynamics is closely similar to that described above for the network response to modulation. The modes may be extracted directly or related to those of the uncoupled population, as required. On considering solutions of the from $P' = P_0' + \hat{P}_\lambda' e^{\lambda t}$, the following two equations describing relaxation to the steady state are found:

$$-\frac{\partial \hat{J}_\lambda'}{\partial V} = \lambda\hat{P}_\lambda' + \hat{r}_\lambda'\delta(V - V_{th}) - \hat{r}_\lambda' e^{-\lambda\tau_r}\delta(V - V_{re}) \tag{49}$$

$$-\frac{\partial \hat{P}_\lambda'}{\partial V} = \frac{1}{\sigma^2}\Big(\tau\hat{J}_\lambda' + (V - E_0' - \psi)\hat{P}_\lambda' - \hat{r}_\lambda' E_s\hat{s}_\lambda P_0'\Big) \tag{50}$$

where $\hat{s}_\lambda$ is the synaptic modulation given in equation (41) with $i\omega \to \lambda$. Hence, the steady-state solution for P_0' is first found and then the set of allowable modes $\{\lambda\}$ are those that provide solutions that, when $\hat{J}_\lambda'$ and $\hat{P}_\lambda'$ are integrated from threshold V_{th} to V_{lb}, satisfy the condition $\hat{J}_\lambda'(V_{lb}) = 0$. These can be computed directly

from the equation pair (49,50) by introducing $\hat{J}'_\lambda = \hat{r}'_\lambda \hat{j}'_\lambda$ and $\hat{P}'_\lambda = \hat{r}'_\lambda \hat{p}'_\lambda$ and scanning over some range of λ (in the complex plane) until all the zeros of $\hat{J}'_\lambda(V_{lb})$ are found.

Relation to the properties of the uncoupled population. Alternatively, the properties of the recurrent network can be related back to the uncoupled population. Equation pair (49,50) can be solved by constructing solutions from the uncoupled case calculated with E_0 replaced by E'_0. On comparison with the uncoupled population subject to current modulation, given by equation pair (30,31), it can be seen that an effective modulation $E'_1 = \hat{r}'_\lambda E_s \hat{s}_\lambda$ can be conveniently defined. Then, on using the relation in equation (37) it is immediately seen that

$$1 = E_s \tau_s \frac{e^{-\lambda \tau_d}}{1 + \lambda \tau_s} \hat{A}(\lambda) \tag{51}$$

where $\hat{A}(\lambda)$ is the response amplitude calculated from equation pair (30,31) with $i\omega$ replaced by λ.

Phase diagram for an inhibitory EIF network. The asynchronous, steady firing state of the network will become unstable to growing oscillations when the real part of the least negative mode vanishes. This occurs when $\lambda = i\omega$ and so the critical condition is given by

$$1 = E_s \tau_s \frac{e^{-i\omega \tau_d}}{1 + i\omega \tau_s} \hat{A}(i\omega). \tag{52}$$

This is equivalent to the self-consistent phase and amplitude criteria already identified (Brunel and Wang 2003) in the context of network oscillations. In figure 3E this relation is used to calculate the critical line for the onset of an oscillatory instability, generalizing part of the analysis of LIF inhibitory networks (Brunel and Hakim 1999) to the non-linear EIF case. The filled circles mark the position of the network response to current modulations that were shown in panels 3Bi-iv. The open circle marks the critical coupling strength, $E^*_s \tau_s r'_0 = -20.3$mV at which spontaneous oscillations appear (for a network rate of $r'_0 = 5.3$Hz). This is the same value of the synaptic coupling at which the amplitude of the resonance peak in response to current modulation diverges. This is as expected, as seen from comparing the denominator of equation (47) with the criticality condition of equation (52).

5 Discussion

In this paper a threshold-integration method, introduced in Richardson (2007) was extended to the calculation of first-passage times and spike-train spectra, as well as the first-order response properties of recurrent networks and their phase diagrams. The implementation of the method is trivial algorithmically, regardless of the complexity of the non-linear IF model in question. It is hoped, therefore, that the method will provide a useful tool for the further analysis of the computational properties of neural tissue at increasing levels of biophysical realism. Before ending the paper, some obvious or desirable extensions of the methods are briefly examined.

Conductance-based network effects. For reasons of clarity, a current-based model of the network coupling was used to illustrate the application of the method to recurrent networks. Synaptic current is conductance-mediated and hence a more realistic model would be to treat the coupling as a conductance modulation $G_S(t)$ with a resulting synaptic current of the form $G_S(t)(E_S - V)$, where E_S is the synaptic reversal potential. The only (minor) complication in this case is finding the self-consistent solution for the steady state which, because of the rate-dependent conductance, would involve the definition of an effective time constant τ' (and potentially an effective noise strength σ' and spike-onset V'_T). However, once a stable fixed point of the network is identified, the effects of conductance modulation can be parameterized by the conductance analogue $\hat{A}_G(i\omega)$ of equation (37). This was previously treated in Richardson (2007) for the uncoupled population, and the results can be directly incorporated into the network context and combined with current modulation, as required. The role of feedback conductance in recurrent networks is largely unexplored and could conceivably lead to some novel oscillatory modes in which conductance-increase periodically shunts the external fluctuations and reduces firing.

Voltage-activated currents. Neurons express class-specific sets of voltage-gated currents, each with their characteristic dynamics. Such currents can give rise to non-passive subthreshold responses and spike-frequency adaptation. Generalizations of leaky IF neurons have been developed that include additional state variables that capture subthreshold dynamics under a linear approximation (Richardson et al. 2003; Brunel et al. 2003) or adaptation currents (Gigante et al. 2007). The linearization approach to subthreshold currents is unlikely to always be valid for non-linear IF neurons because the explicit spike covers a significant voltage range. A further development of the boundary integration framework to incorporate additional state variables, for generalised non-linear IF neurons, would be desirable. Though this would require going beyond the one-dimensional treatment developed here, it would allow for the description of a considerably wider range of neuronal response properties.

Synaptic shot noise. Finally, it has recently be pointed out (Hohn and Burkitt 2001; Richardson and Gerstner 2005, 2006; Wolff and Lindner 2008) that the effects of synaptic shot noise coming from the finite-sized amplitude of post-synaptic potentials, and which are neglected in the diffusion approximation, can have a significant impact on the voltage distributions and firing properties of neurons. The boundary integration method relies on

the presence of a first-order derivative of the probability density in the current equation (5) which comes directly from the diffusive, gaussian white-noise term. Hence, it can be expected that any attempt to account for synaptic shot-noise will not fall directly into the present framework. However, given that the non-gaussian nature of synaptic drive is becoming of increasing interest experimentally (DeWeese and Zador 2006) a similar framework for shot noise would be worth pursuing.

Appendix

5.1 Implementation of the algorithm.

The threshold-integration method involves integrating pairs of equation of the form (9,10), backwards from V_{th} to a lower bound V_{lb}. These pairs of equations have the same features; an equation with a derivative of flux J that also contains initial and boundary conditions (in the form of Dirac delta-functions), and an equation with a derivative of probability density P. The equations can be solved by integrating from threshold to a lower bound V_{lb}. A discretization of voltage into $n{+}1$ steps $k{=}0, 1, \cdots n$ of size Δ such that $V^{(k)} = V_{lb} + k\Delta$ and $V^{(n)} = V_{th}$ is made. It is convenient to choose Δ so that the reset V_{re} falls on a lattice point k_{re}.

The pairs of equations for J and P must be solved simultaneously (i.e. within the same loop over k from n to 0). However, the integration scheme suggested here is different for the J and P equations. A convenient method for integrating the two is now described with the population current-modulation equations (33,34) and (35,36) - four first-order differential equations in total - used as an example.

Integrating J equations. The flux equation (33) for $\hat{\jmath}_r$ contains Dirac-delta functions at reset and threshold. The delta function at threshold is accounted for by choosing the initial conditions $\hat{\jmath}_r^{(n)}{=}1$, and the delta function at reset appears as a Kronecker delta function $\delta_{k,k_{re}+1}$ which is equal to one if $k = k_{re} + 1$, but zero otherwise. Hence for $\hat{\jmath}_r$ the iteration is

$$\hat{\jmath}_r^{(k-1)} = \hat{\jmath}_r^{(k)} + \Delta i\omega\hat{p}_r^{(k)} - e^{-i\omega\tau_r}\delta_{k,k_{re}+1} \tag{53}$$

with initial condition $\hat{\jmath}_r^{(n)}{=}1$. The equation for $\hat{\jmath}_E$ does not feature any sink or source delta functions so the iteration is simply

$$\hat{\jmath}_E^{(k-1)} = \hat{\jmath}_E^{(k)} + \Delta i\omega\hat{p}_E^{(k)} \tag{54}$$

with initial condition $\hat{\jmath}_E^{(n)} = 0$.

Integrating the P equations. The equations with derivatives of P require more care because of the large values that the spike-generating current $\psi(V)$ can take. A simple method that avoids the problems associated with this is to note first that the equations for P are all of the form

$$-\left(\frac{dP}{dV} + G(V)P(V)\right) = H(V) \tag{55}$$

where $H(V)$ is in general some function of voltage, flux and steady-state densities, and where

$$G(V) = \frac{V - E_0 - \psi}{\sigma_V^2}. \tag{56}$$

Equation (55) can be rearranged and integrated between voltage steps $k{-}1$ and k

$$-\frac{d}{dV}\left(P(V)e^{\int^V G(W)dW}\right) = H(V)e^{\int^V G(W)dW} \tag{57}$$

so that

$$P^{(k-1)} = P^{(k)}e^{\int_{V^{(k-1)}}^{V^{(k)}} G(W)dW} + \int_{V^{(k-1)}}^{V^{(k)}} dW H(W)e^{\int_{V^{(k-1)}}^{W} G(W')dW'} \tag{58}$$

which is exact. This can now be approximated to give the value $P^{(k-1)}$ as a function of quantities evaluated at the early step k, thus

$$P^{(k-1)} \simeq P^{(k)}e^{\Delta G^{(k)}} + \int_{V^{(k-1)}}^{V^{(k)}} dW H^{(k)}e^{G^{(k)}(W - V^{(k-1)})} \tag{59}$$

$$P^{(k-1)} \simeq P^{(k)}e^{\Delta G^{(k)}} + H^{(k)}\frac{(e^{\Delta G^{(k)}} - 1)}{G^{(k)}} \tag{60}$$

where for all cases $P^{(n)}{=}0$ provides the initial condition. For equations (34) and (36) the quantities $H^{(k)}$ are

$$H_r^{(k)} = \frac{\tau\hat{\jmath}_r^{(k)}}{\sigma^2} \quad \text{and} \quad H_E^{(k)} = \frac{\tau\hat{\jmath}_E^{(k)} - P_0^{(k)}}{\sigma^2} \tag{61}$$

respectively, and where $P_0^{(k)}$ is the steady-state solution (found from applying the method first to Eqs. 9,10).

Extracting the rate. For time-dependent quantities the rate is found from the zero-flux condition given in equation (37) so that $\hat{r}_E = -E_1\hat{\jmath}_E^{(0)}/\hat{\jmath}_r^{(0)}$. However, for the steady state the rate is found from normalizing the distribution p_0 as described in equation (11).

Time step. An integration step-size of 10μV was sufficiently accurate for generating the figures used in this paper. For frequencies considerably higher than 1000Hz in combination with weak noise σ_V a smaller step might be required for convergence.

Availability of the code. The resulting code required to generate the flux and probability densities is simple (in general only a few tens of lines). The MATLAB programs for cases considered in this paper are freely available from the author on request.

5.2 Fourier transform convention.

The fourier transform of $Y(t)$ and its inverse $\widetilde{Y}(\omega)$ are defined asymmetrically as

$$\widetilde{Y}(\omega) = \int_{-\infty}^{\infty} dt Y(t) e^{-i\omega t} \text{ and } Y(t) = \int_{-\infty}^{\infty} \frac{d\omega}{2\pi} \widetilde{Y}(\omega) e^{i\omega t}.$$

5.3 Stochastic simulations.

All simulations were performed in the MATLAB environment with a time step $dt = 0.1$ms or smaller using a first-order forward Euler method. Network simulations comprised at least 5,000 neurons. During the refractory period τ_r, which is measured from the time of the spike peak at V_{th}, the fall of the spike was explicitly modeled as a piecewise exponential function

$$V_1 = A_0 - A_1 e^{(t-t^*)/\tau_1} \quad \text{for } 0 < t < t^*$$
$$V_2 = B_0 + B_1 e^{(t^*-t)/\tau_2} \quad \text{for } t^* < t < \tau_r$$

with the spike peak at a relative time $t = 0$. The voltage and its gradient are matched at an intermediate time t^* to fix the constants as

$$A_1 = \frac{(V_{th} - V_{re})\tau_1}{\tau_2(1 - e^{(t^*-\tau_r)/\tau_2}) + \tau_1(1 - e^{-t^*/\tau_1})} \quad (62)$$

and $B_1 = A\tau_2/\tau_1$, $A_0 = V_{th} + A_1 e^{-t^*/\tau_1}$, $B_0 = V_{re} - B_1 e^{(t^*-\tau_r)/\tau_2}$. For this paper the parameters chosen to model the fall of the spike were $\tau_1 = 1$ms, $\tau_2 = 2$ms, $t^* = 2$ms and $\tau_r = 10$ms. Clearly for the case of the non-linear integrate-and-fire models considered here the post-spike refractory behavior is purely decorative; the refractory period could be modeled as having the voltage (non-biophysically) fixed at V_{re}, for example. However, more generally, if a voltage-activated current were to be included, then the shape of the spike can potentially play an important role. This is particularly the case for currents that activate or deactivate over the range of the spike.

Acknowledgements The author acknowledges funding from the Research Councils United Kingdom (RCUK) with whom he holds an Academic Fellowship.

References

Arsiero M, Lüscher H-R, Lundstrom BN and Giugliano M (2007) The impact of input fluctuations on the frequency-current relationships of layer 5 pyramidal neurons in the rat medial prefrontal cortex. J Neurosci. 27:3274-3284.

Badel L, Lefort S, Brette R, Petersen CCH, Gerstner W, and Richardson MJE (2008) Dynamic I-V curves are reliable predictors of naturalistic pyramidal-neuron voltage traces. J. Neurophysiol. 99:656-666

Brunel N and Hakim V (1999) Fast Global Oscillations in Networks of Integrate-and-Fire Neurons with Low Firing Rates. Neural Comput. 11:1621-1671.

Brunel N and Wang X-J (2003). What determines the frequency of fast network oscillations with irregular neural discharges? Journal of Neurophysiology, 90:415-430.

Brunel N and Latham P (2003). Firing rate of noisy quadratic integrate-and-fire neurons. Neural Computation 15:2281-2306.

Brunel N, Hakim V and Richardson MJE (2003) Firing-Rate Resonance in a Generalized Integrate-and-Fire Neuron with Subthreshold Resonance. Phys Rev E 67: art-no 051916.

Burkitt AN (2006a) A review of the integrate-and-fire neuron model: I. Homogeneous synaptic input. Biol. Cybern. 95:1-19.

Burkitt AN (2006b) A review of the integrate-and-fire neuron model: II. Inhomogeneous synaptic input and network properties. Biol. Cybern. 95: 97-112.

Ermentrout GB and Kopell N (1986) Parabolic bursting in an excitable system coupled with a slow oscillation. SIAM J. Appl. Math. 46:233-253.

Fourcaud-Trocmé N, Hansel D, van Vresswijk C and Brunel N (2003) How Spike Generation Mechanisms Determine the Neuronal Response to Fluctuating Inputs. J. Neurosci. 23:11628-11640.

Fourcaud-Trocmé N and Brunel N (2005) Dynamics of the instantaneous firing rate in response to changes in input statistics. J. Comput. Neurosci. 18:311-321

Fuhrmann G, Markram H and Tsodyks M (2002) Spike Frequency Adaptation and Neocortical Rhythms. J. Neurophys. 88:761-770.

Gerstner W and Kistler WM (2002) Spiking Neuron Models, Cambridge University Press.

Gigante G, Mattia M and Del Giudice P (2007) Diverse Population-Bursting Modes of Adapting Spiking Neurons. Phys. Rev. Lett. 98: art-no 148101.

Hodgkin A and Huxley A (1952) A quantitative description of membrane current and its application to conduction and excitation in nerve. J. Physiol. 117:500-544.

Hohn N and Burkitt AN (2001) Shot noise in the leaky integrate-and-fire neuron. Phys. Rev. E. 63:art-no 031902.

Johannesma PIM (1968) In *Neural networks* (ER Caianiello, ed.) pp. 116-144 (Springer, New York.

Jolivet A, Rauch A, Lüscher H-R, Gerstner W (2006)Predicting spike timing of neocortical pyramidal neurons by simple threshold models. J Comput Neurosci 21:35-49.

Jolivet R, Kobayashi R, Rauch A, Naud R, Shinomoto S and Gerstner W (2008) A benchmark test for a quantitative assessment of simple neuron models. J. Neurosci. Methods 169: 417-424.

Knight BW (1972a) Dynamics of Encoding in a Population of Neurons. J. Gen. Physiol. 59:734-766.

Knight BW (1972b) The Relationship between the Firing Rate of a Single Neuron and the Level of Activity in a Population of Neurons. J. Gen. Physiol. 59:767-778.

Köndgen H, Geisler C, Fusi S, Wang X-J, Lüscher H-R, and Giugliano M (2008). The dynamical response properties of neocortical neurons to temporally modulated noisy inputs in vitro. Cerebral Cortex, doi:10.1093/cercor/bhm235.

Lansky P and Lanska V (1987) Diffusion approximation of the neuronal model with synaptic reversal potentials. Biol. Cybern. 56:19-26.

Lindner B and Schimansky-Geier L (2001) Transmission of noise coded versus additive signals through a neuronal ensemble. Phys. Rev. Lett. 86:2934-2937.

Lindner B, Schimansky-Geier L and Longtin A (2002) Maximizing spike train coherence or incoherence in the leaky integrate-and-fire model. Phys. Rev. E 66: art-no. 031916.

Lindner B, Longtin A and Bulsara A (2003) Analytic expressions for rate and CV of a type I Neuron driven by white Gaussian noise. Neural Comput. 15:1761 - 1788 .

Lindner B, Garcia-Ojalvo J, Neiman A, and Schimansky-Geier L (2004) Effects of noise in excitable systems. Phys. Reports 392:321-424.

Paninski L, Pillow JW, Simoncelli EP (2004) Maximum likelihood estimation of a stochastic integrate-and-fire neural encoding model. Neural Comput 16:2533-2561, 2004.

Rauch A, La Camera G, Luscher H-R, Senn W and Fusi S (2003) Neocortical Pyramidal Cells Respond as Integrate-and-Fire Neurons to In Vivo Like Input Currents. J. Neurophys. 90:1598-1612.

Ricciardi LM (1977) Diffusion processes and related topics in biology Springer, Berlin Heidelberg, New York.

Richardson MJE, Brunel N and Hakim V (2003) From Subthreshold to Firing-Rate Resonance. J. Neurophysiol. 89:2538-2554.

Richardson MJE (2004) Effects of Synaptic Conductance on the Voltage Distribution and Firing Rate of Spiking Neurons. Phys. Rev. E 69: art-no 051918.

Richardson MJE and Gerstner W (2005) Synaptic shot noise and conductance fluctuations affect the membrane voltage with equal significance. Neural Comput. 17:923-947.

Richardson MJE and Gerstner W (2006) Statistics of subthreshold neuronal voltage fluctuations due to conductance-based synaptic shot noise. Chaos 16: art-no 026106.

Richardson MJE (2007) Firing-rate response of linear and nonlinear integrate-and-fire neurons to modulated current-based and conductance-based synaptic drive. Phys. Rev. E 76: article-no 021919.

Risken H (1996) The Fokker-Planck Equation. Springer-Verlag, Berlin, Heidelberg, New York.

Silberberg G, Bethge M, Markram H, Pawelzik K and Tsodyks M (2004) Dynamics of Population Rate Codes in Ensembles of Neocortical Neurons. J. Neurophysiol. 91:704-709.

Stein RB (1965) A theoretical analysis of neuronal variability. Biophys. J. 5:173-194.

DeWeese MR and Zador AM (2006) Non-Gaussian Membrane Potential Dynamics Imply Sparse, Synchronous Activity in Auditory Cortex. J. Neurosci. 26:12206-12218.

Wolff L and Lindner B (2008) Method to calculate the moments of the membrane voltage in a model neuron driven by multiplicative filtered shot noise. Phys. Rev. E 77: article-no 041913.